NeuroImage: Clinical 23 (2019) 101875

Contents lists available at ScienceDirect

NeuroImage: Clinical

journal homepage: www.elsevier.com/locate/ynicl

Structural anomaly in the reticular formation in narcolepsy type 1, suggesting lower levels of neuromelanin

Natasha Morales Drissi[a,b], Marcel Warntjes[a,b], Alexander Wessén[c], Attila Szakacs[d], Niklas Darin[d], Tove Hallböök[d], Anne-Marie Landtblom[b,e,f], Helena Gauffin[e], Maria Engström[a,b,*]

[a] Department of Medical and Health Sciences (IMH), Linköping University, 581 83 Linköping, Sweden
[b] Center for Medical Image Science and Visualization, Linköping University, 581 83 Linköping, Sweden
[c] Linköping University, 581 83 Linköping, Sweden
[d] Department of Pediatrics, Queen Silvia Children's Hospital, Institute of Clinical Sciences, The Sahlgrenska Academy at the University of Gothenburg, 416 50 Gothenburg, Sweden
[e] Department of Clinical and Experimental Medicine (IKE), Linköping University, 581 83 Linköping, Sweden
[f] Department of Neuroscience, Uppsala University, 752 36 Uppsala, Sweden

ARTICLE INFO

Keywords:
Quantitative MRI (qMRI)
Relaxation time
Myelin
Neuromelanin
Orexin/hypocretin
Locus coeruleus

ABSTRACT

The aim of this study was to investigate structural changes in the brain stem of adolescents with narcolepsy, a disorder characterized by excessive daytime sleepiness, fragmented night-time sleep, and cataplexy. For this purpose, we used quantitative magnetic resonance imaging to obtain R1 and R2 relaxation rates, proton density, and myelin maps in adolescents with narcolepsy ($n = 14$) and healthy controls ($n = 14$). We also acquired resting state functional magnetic resonance imaging (fMRI) for brainstem connectivity analysis. We found a significantly lower R2 in the rostral reticular formation near the superior cerebellar peduncle in narcolepsy patients, family wise error corrected $p = .010$. Narcolepsy patients had a mean R2 value of $1.17\,s^{-1}$ whereas healthy controls had a mean R2 of $1.31\,s^{-1}$, which was a large effect size with Cohen d = 4.14. We did not observe any significant differences in R1 relaxation, proton density, or myelin content. The sensitivity of R2 to metal ions in tissue and the transition metal ion chelating property of neuromelanin indicate that the R2 deviant area is one of the neuromelanin containing nuclei of the brain stem. The close proximity and its demonstrated involvement in sleep-maintenance, specifically through orexin projections from the hypothalamus regulating sleep stability, as well as the results from the connectivity analysis, suggest that the observed deviant area could be the locus coeruleus or other neuromelanin containing nuclei in the proximity of the superior cerebellar peduncle. Hypothetically, the R2 differences described in this paper could be due to lower levels of neuromelanin in this area of narcolepsy patients.

1. Introduction

Narcolepsy is a chronic sleep disorder, characterized by excessive daytime sleepiness with frequent uncontrollable sleep attacks (Dauvilliers et al., 2003; Silber et al., 2002). Other symptoms include sleep abnormalities such as sleep paralysis, hypnagogic (upon falling asleep) or hypnopompic (upon awakening) hallucinations, and nocturnal dyssomnia with fragmented sleep and frequent awakenings. Most narcolepsy patients also suffer from cataplexy, a sudden reduction or loss of muscular tone not accompanied by a loss of consciousness (Aran et al., 2010; Peraita-Adrados et al., 2011). The symptoms in narcolepsy type 1 are caused by impaired hypocretin/orexin (OX) signaling (Lin et al., 1999; Thannickal et al., 2000) and can be induced experimentally in canine or murine models by mutations to the hypocretin/OX genes (Blumberg et al., 2007; Hungs et al., 2001). While most human narcolepsy is non-familial and no associated hypocretin/OX mutations have been discovered, patients have an 85%–95% reduction in the number of OX neurons as well as abnormally low levels of OX in the CSF (Thannickal et al., 2000; Khatami et al., 2004). OX neurons are found exclusively within the lateral hypothalamic and the perifornical areas but project widely throughout the brain and the spinal cord. Orexinergic projections to several wake-promoting areas such as the ventral tegmental area (VTA), locus coeruleus (LC), and other neuronal populations of the brainstem (Dergacheva et al., 2016; Espana et al.,

Abbreviations: DRN, dorsal raphe nucleus; LC, locus coeruleus; PD, proton density; SMA, supplementary motor area

* Corresponding author at: CMIV, Linköping University/US, 581 83 Linköping, Sweden.
E-mail address: maria.engstrom@liu.se (M. Engström).

https://doi.org/10.1016/j.nicl.2019.101875
Received 14 November 2018; Received in revised form 4 April 2019; Accepted 25 May 2019
Available online 29 May 2019

2005; Horvath et al., 1999) have also been confirmed.

While narcolepsy patients have reduced numbers of OX neurons, no clear radiological evidence of macroscopic lesions specific to narcolepsy have been discovered in sporadic patients (Frey and Heiserman, 1997). Voxel-based morphometry based on T1 weighted magnetic resonance imaging (MRI), however, shows a reduction of grey matter in the hypothalamus, amygdala, and the hippocampus of narcolepsy patients (Weng et al., 2015). In addition, other studies using diffusion tensor imaging (DTI) found widespread white matter changes encompassing several white matter tracts (Juvodden et al., 2018) including areas of the brainstem such as the hypothalamus, VTA, dorsal raphe, mesencephalon, pons, and the medulla oblongata (Menzler et al., 2012). For a comprehensive overview of previous neuroimaging in narcolepsy we refer to recent reviews (Weng et al., 2015; Wada et al., 2019). The lack of consistent findings of brain structural anomalies in narcolepsy might be attributed to insufficiently sensitive imaging methods.

Here, we apply quantitative MRI (qMRI) to acquire maps of R1 and R2 relaxation rates and proton density (PD) in one single scan, which can characterize tissue properties on an absolute scale. Moreover, these quantitative parameters can be used to calculate myelin content in each image voxel (Warntjes et al., 2017; Warntjes et al., 2016). Such quantitative parameter and myelin maps are very sensitive to minor pathological variants and to our knowledge no previous study has analyzed brain structure in narcolepsy patients using qMRI.

This paper is published as part of a larger project aiming to reveal fundamental physiological mechanisms in narcolepsy (Drissi et al., 2016; Witt et al., 2018) as well as to identify possible MRI biomarkers for narcolepsy. Structural brain imaging studies on narcolepsy have discovered small changes to structures in the brainstem and the midbrain involved in the signaling pathways of OX, however due to technological advancements in the field of neuroimaging as well as updated diagnostic criteria many of the results from these studies may need to be revisited. The aim of this paper was to investigate brainstem structure in narcolepsy patients using qMRI. Specifically, we aimed to investigate potential differences between narcolepsy patients and healthy controls regarding structures associated with OX neuronal projections in the brainstem.

2. Materials and methods

2.1. Patients

Twenty-one participants with narcolepsy type 1 were recruited from a population-based study in western Sweden ($n = 15$) (Szakacs et al., 2013) and from paediatric clinics in the county of Östergötland ($n = 6$). Diagnoses were based on the classification codes of the Swedish version of the International Classification of Diseases, Tenth Revision (ICD-10) and the diagnostic criteria for narcolepsy according to the International Classification of Sleep Disorders – Second Edition (ICSD-2, 2005) (Medicine AAoS, 2005) and Third Edition (ICSD-3, 2014) (Medicine AAoS, 2014). All patients but one got narcolepsy after H1N1 (Pandemrix) vaccination. Inclusion criteria for patients were a confirmed diagnosis of narcolepsy and being between 12 and 20 years of age at time of enrolment. Patients were excluded if there was evidence of cognitive disabilities. Narcolepsy patients were allowed to take their prescribed medications prior to the exam.

For the qMRI analysis, data from seven narcolepsy patients were excluded from further analyses due to equipment malfunction and/or severe image artefacts. This left a final sample size of 14 participants with narcolepsy for the qMRI data. CSF orexin status (< 130 pg/ml) was taken at time of diagnosis for all but six patients (Table 1). Data from the narcolepsy patients were compared to 14 age and sex matched healthy controls, which were recruited by advertisement. Controls were confirmed to have no medical history of neuropathological diseases or mental illness by questionnaires and interviews prior to examination.

In addition to qMRI, we also acquired resting state functional MRI (fMRI) data in order to investigate the functional connectivity of eventual brainstem anomalies. For the connectivity analysis two of the patients that had been excluded from the qMRI analysis could be included, leaving a final sample of 16 narcolepsy patients and 14 controls. The Regional ethical review board in Linköping, Sweden, approved the study (2013/99-31) and all participants gave written informed consent to participate in accordance with the declaration of Helsinki. For all participants under the age of 16, written informed consent was obtained from the parents.

2.2. Procedure

All participants were monitored with actigraphy (Sense Wear, Body Media, Inc. Pittsburgh, PA, USA) using an armband with an actigraphy device mounted on the back of the left upper arm. The participants carried the device approximately 23 h each day during one week before the MRI examination. The actigraphy device contained a multisensory array including a 3-axis accelerometer, heat flux sensor, galvanic skin response sensor (GSR), and a skin temperature sensor. Algorithms taking these multisensory measures into account give estimates of *e.g.,* daily sleep duration and sleep efficacy.

Participants were asked to fill in a questionnaire based on the Stanford Sleep Inventory (http://www.stanfordhealthcare.org) that contained seven questions about cataplexy-related symptoms (range 0–5 for each question; 0–35 total range) and the Epworth sleepiness scale (ESS) with questions about tendencies to fall asleep in different daily situations (range 0–24). Following ranges are approximate sleepiness evaluations from ESS: 0–5 Lower normal daytime sleepiness; 6–10 Higher normal daytime sleepiness; 11–12 Mild excessive daytime sleepiness; 13–15 Moderate excessive daytime sleepiness: 16–24 Severe excessive daytime sleepiness. All participants also indicated their levels of fatigue, depression, anxiety, and sleepiness at the time of MRI on a visual analogue scale (VAS), where 0 indicated no sign of these symptoms and 100 indicated highest possible degree.

2.3. MRI

All MR images were acquired on a Philips Achieva 3 Tesla MRI scanner (Philips Healthcare, Best, Netherlands). Quantitative MRI was used to acquire R1, R2, and PD maps, which were used to calculate the myelin maps and also synthetic T2 weighted images used for image normalization. The MR quantification was performed using a multi-dynamic multi-echo (MDME) sequence, where 8 images per slice at 4 saturation delays and 2 echo times are acquired in parallel. The saturation delay times were 135, 535, 1865, and 3865 ms at a repetition time (TR) of 4000 ms. The echo times (TE) were 13 and 100 ms. All 8 images have different effects of R1 and R2 relaxation rates, which enables the measurement of R1, R2, and PD. The field of view (FOV) was 230×190 mm, the resolution was 0.8 mm in plane, slice thickness 5 mm, gap 1 mm, 30 slices. The scan time was 6 min and 8 s. Details of the sequence are described by Warntjes et al. (Warntjes et al., 2008). Post-processing of the maps was performed by SyMRI 8.0.4 (SyntheticMR, Linköping, Sweden). Post-processing time was about 10 s on a regular laptop.

Resting state fMRI images were acquired using a 32-channel head coil with a single-shot, gradient-echo, echo-planar imaging (EPI) sequence with following scanner parameters: TR = 2200 ms; TE = 35 ms; flip angle = 77°; FOV = 240×240 mm; matrix = 80×80; voxel size: $3 \times 3 \times 3$ mm^3 (no slice gap, full brain coverage); SENSE factor = 2; total scan time = 10 min. During the resting-state scan, participants were instructed to lie still with their eyes closed and given no special instructions to stay awake. High resolution T1 weighted images were used for fMRI image normalization and these images were also reviewed by a radiologist to ensure that the participants were free from any obvious pathologic abnormalities.

Table 1
Narcolepsy patient demographics.

Patient	Gender	Age (y)	Narcolepsy duration (y)	CSF-orexin (pg/ml)	Medications
				< 130 pg/ml	
1	F	17	6	81	Methylphenidate, fluoxetine
2	M	17	5	< 10	Methylphenidate, sodium oxybate
3	F	18	5	< 10	Methylphenidate, modafinil, fluoxetine
4	F	19	4	79	None
5	M	14	9	< 10	Methylphenidate
6	M	19	4	49	Methylphenidate
7	F	20	5	Unknown	Methylphenidate, sertraline
8	F	19	4	18	None
9	F	16	4	130	Methylphenidate, fluoxetine, levothyroxine
10	F	19	5	Unknown	Modafinil
11	M	16	4	Unknown	Methylphenidate, fluoxetine
12	F	15	4	Unknown	Modafinil, fluoxetine
13	F	18	5	Unknown	Methylphenidate, fluoxetine
14	F	17	5	< 10	Methylphenidate, fluoxetine, zolpidem

2.4. qMRI image analysis

After exclusion of participants due to artefacts, the R1, R2, PD, and myelin images of 14 patients and 14 healthy controls were normalized to a standardized brain in Montreal Neurological Institute (MNI) coordinates using SPM12 (Statistical Parametric Mapping, http://www.fil.ion.ucl.ac.uk/spm/software/spm12). Before running the normalization protocol in SPM12, each image was reoriented so that the origin was set at the anterior commissure. The default tissue probability map for normalization in SPM12 was used, and voxel size for the written normalized images were set to be the same as the input data, which was 0.898 × 0.898 × 5 (x, y and z in mm). Normalized, unsmoothed images were used for statistical analysis of differences in the brainstem between the narcolepsy group and the control group. This analysis was done with a two-sample *t*-test implemented in SPM12. Age and sex were added as covariates in the analysis. A brainstem image mask from Wake Forrest University's (WFU) Pickatlas was used to limit the analysis results to the brainstem (Fig. 1 A–C). The nature of the mask was set to be inclusive, with no *p*-value adjustment and 0 extent threshold. The small volume correction function of SPM12 was used to correct the *p*-values of the analysis to the volume defined by the brainstem image mask, using family wise error (FWE) correction for multiple comparisons. The FWE correction was made with regards to the number of voxels, # = 4819, within the brainstem mask for each qMRI map separately.

In addition to the primary brainstem analysis, we investigated eventual R2 differences in predefined regions of interest (ROIs) in *post hoc* analyses. These regions were based on Bär et al. (Bar et al., 2016). The locus coeruleus (LC) was defined as a box with dimensions $4 \times 6 \times 10\,mm^3$ centered at MNI coordinates [−5–34 -21] and [7–34 -21] for the left and right LC, respectively (# voxels = 45). The dorsal Raphe nucleus (DRN) was defined as a sphere with radius 4 mm centered at MNI coordinates [2–26 -18] (# voxels = 33).

2.5. Functional connectivity analysis

We performed seed-to-voxel functional connectivity analysis in order to aid the anatomical localization of findings from the quantitative MRI. The seed region was created from significant R2 group differences in the brain stem, see Results section 3.2. Resting state fMRI data from 16 narcolepsy patients and 14 controls were preprocessed and analyzed using the CONN functional connectivity toolbox (Whitfield-Gabrieli and Nieto-Castanon, 2012) (http://www.nitrc.org/projects/conn). Image preprocessing was made using the standard pipeline in CONN with realignment for estimation and correction of motion during scanning; unwarping for estimation and removal of movement-by-susceptibility induced variance in the fMRI time series; slice timing correction, outlier detection and scrubbing; segmentation of the T1W images into grey matter, white matter, and CSF as

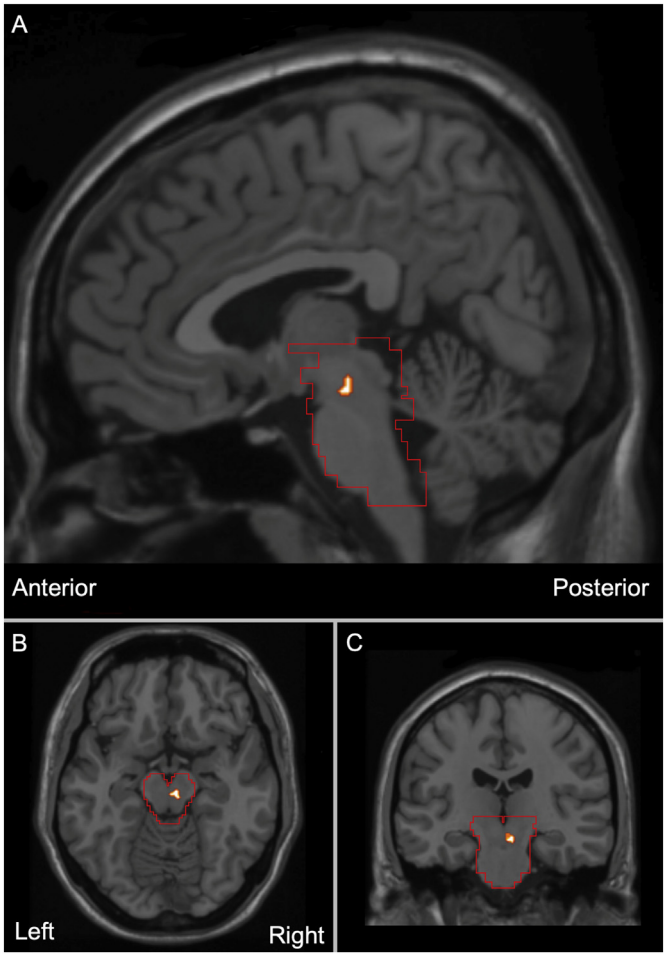

Fig. 1. Lower R2 values in narcolepsy. The figures show statistically significant R2 differences between narcolepsy patients and healthy controls in sagittal (A), axial (B) and coronal (C) planes. Narcolepsy patients had significantly lower R2 than controls in the rostral reticular formation adjacent to the superior cerebellar peduncle, peak coordinates = [2–22 -14]. The images are shown with an uncorrected threshold of $p = .001$. The red contours represent the brainstem mask used for small volume correction. (For interpretation of the references to color in this figure legend, the reader is referred to the web version of this article.)

preparation for normalization of the functional images to MNI coordinates; smoothing using a Gaussian kernel for spatial convolution to ameliorate intersubject differences in anatomy. A band-pass filter of 0.008–0.09 Hz and linear detrending was used for denoising the functional images. Whole brain functional connectivity of the R2 abnormal region in the brain stem was calculated as bivariate correlation using hemodynamic response weighting. We also compared the functional connectivity of narcolepsy patients and healthy controls using age and sex as covariates in a two-sample *t*-test. Results are reported as significant if false discovery rate (FDR) cluster-size *p*-value, $p_{FDR} < 0.05$ based on a primary height threshold of uncorrected $p < .001$.

2.6. Correlation to clinical measures

Results based on the qMRI data, showed that narcolepsy patients differed from healthy controls regarding the R2 values in a region in the rostral reticular formation, see section 3.2. For further statistical analysis, we extracted each patient's R2 value (s^{-1}) within the resulting region of interest in the brainstem using the eigenvariate function in SPM12, which gives the results as a weighted mean. We also extracted mean values for the predefined regions *i.e.,* bilateral LC and DRN. The R2 values were used to examine relationships to the clinical measures using a linear regression model with the mean R2 value as dependent variable and sleep efficacy, total sleep duration, cataplexy, age, sex, and group (narcolepsy/controls) as independent variables in IBM SPSS Statistics, version 25. We also analyzed R2 data for group*clinical variable interactions to assess potential differential associations between groups.

3. Results

3.1. Results from descriptive statistics

The mean age of our participants was approximately 16.5 years and there was no age difference between narcolepsy and healthy controls (Table 2). Both groups carried the actigraphy device during 6 days in mean. While there was no difference in total daily sleep duration between narcolepsy and controls, the narcolepsy patients had significantly lower sleep efficacy and spent longer time in bed each day. As expected, the narcolepsy patients rated higher on ESS sleepiness and on cataplexy, but there were no group differences in perceived fatigue, depression, anxiety, or sleepiness at the day of MRI.

Table 2
Descriptive statistics of clinical data. The table shows mean values, standard deviations (sd), and two-tailed *p*-values from actigraphy measurements and questionnaires. The actigraphy data "Lying down", "sleep duration", and "sleep efficacy" refer to daily mean. Visual analogue scale (VAS) data for fatigue, depression, anxiety, and sleepiness were collected before MRI. ESS = Epworth sleepiness scale.

Variable	Mean (sd) Narcolepsy	Mean (sd) Healthy controls	p-value
Age (years)	16.4 (2.2)	16.7 (2.1)	0.745
Actigraphy duration (days)	6.0 (1.4)	6.0 (1.0)	1.000
Actigraphy duration (%)	90.7 (6.8)	91.2 (6.6)	0.827
Lying down, (hh:mm/24 h)	9:37 (2:17)	7:55 (0:51)	**0.012**
Sleep duration, (hh:mm/24 h)	6:00 (1:53)	6:29 (0:54)	0.361
Sleep efficacy (%)	63 (15)	82 (6)	< **0.001**
ESS [0–24]	15.9 (3.3)	5.6 (3.5)	< **0.001**
Cataplexy [0–35]	12.1 (7.1)	3.4 (3.1)	< **0.001**
VAS Fatigue [0 − 100]	40.1 (21.8)	37.2 (23.8)	0.743
VAS Depression [0–100]	4.6 (8.2)	5.4 (4.8)	0.760
VAS Anxiety [0–100]	7.6 (10.4)	14.8 (20.2)	0.251
VAS Sleepiness [0–100]	33.1 (25.6)	34.6 (26.8)	0.881

Significant differences between narcolepsy patients and healthy controls are marked with p-values in bold font.

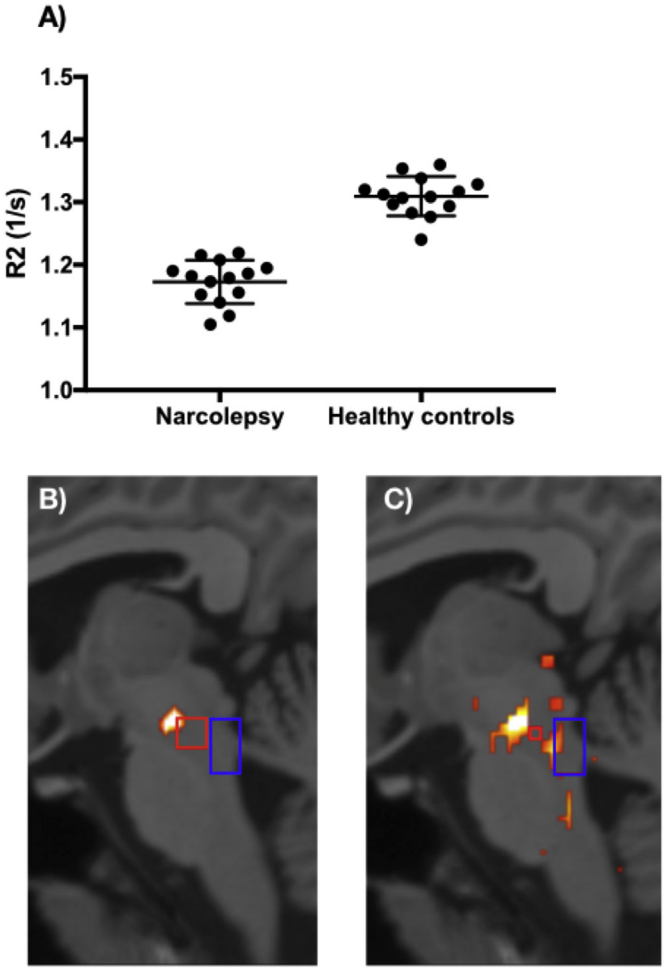

Fig. 2. R2 values in brainstem regions of interest. A) Scatter plot of R2 values from the significant deviant region in the rostral reticular formation showing mean values and standard deviation. B) Brainstem image showing the area where narcolepsy patients had significantly lower R2 compared to controls, also see Fig. 1. The predefined regions of interest are delineated with blue contours for locus coeruleus (LC) and red for the dorsal raphe nucleus DRN according to (Bar et al., 2016). C) Brainstem image showing the results at uncorrected *p*-value threshold of $p = .05$. Predefined regions of interest are shown in blue and red contours for LC and DRN, respectively. (For interpretation of the references to color in this figure legend, the reader is referred to the web version of this article.)

3.2. Significant R2 anomalies in narcolepsy patients

When comparing the R2 maps of narcolepsy patients and healthy controls, we observed that the narcolepsy patients had significantly lower R2 than controls in the rostral reticular formation adjacent to the superior cerebellar peduncle, peak coordinates = [2–22 -14]; FWE corrected peak-level *p*-value = .010 (Fig. 1). Narcolepsy patients had a mean R2 value of 1.17 s^{-1} whereas healthy controls had a mean R2 of 1.31 s^{-1} (Fig. 2A). Cohen d was 4.14, which is regarded as a large effect size (> 0.5). When not including age and sex as covariates in the analysis, narcolepsy patients had significantly lower R2 values in the area corresponding to the peak in the left hemisphere of the brainstem (Supplementary Fig. S1). No significant group differences were found in either of the R1, PD, or myelin images.

In the *post hoc* analysis, we also found R2 differences in the predefined left LC, uncorrected $p_{unc} = 0.005$, right LC, $p_{unc} = 0.011$, and DRN, $p_{unc} = 0.006$. In all three cases, narcolepsy patients had lower R2

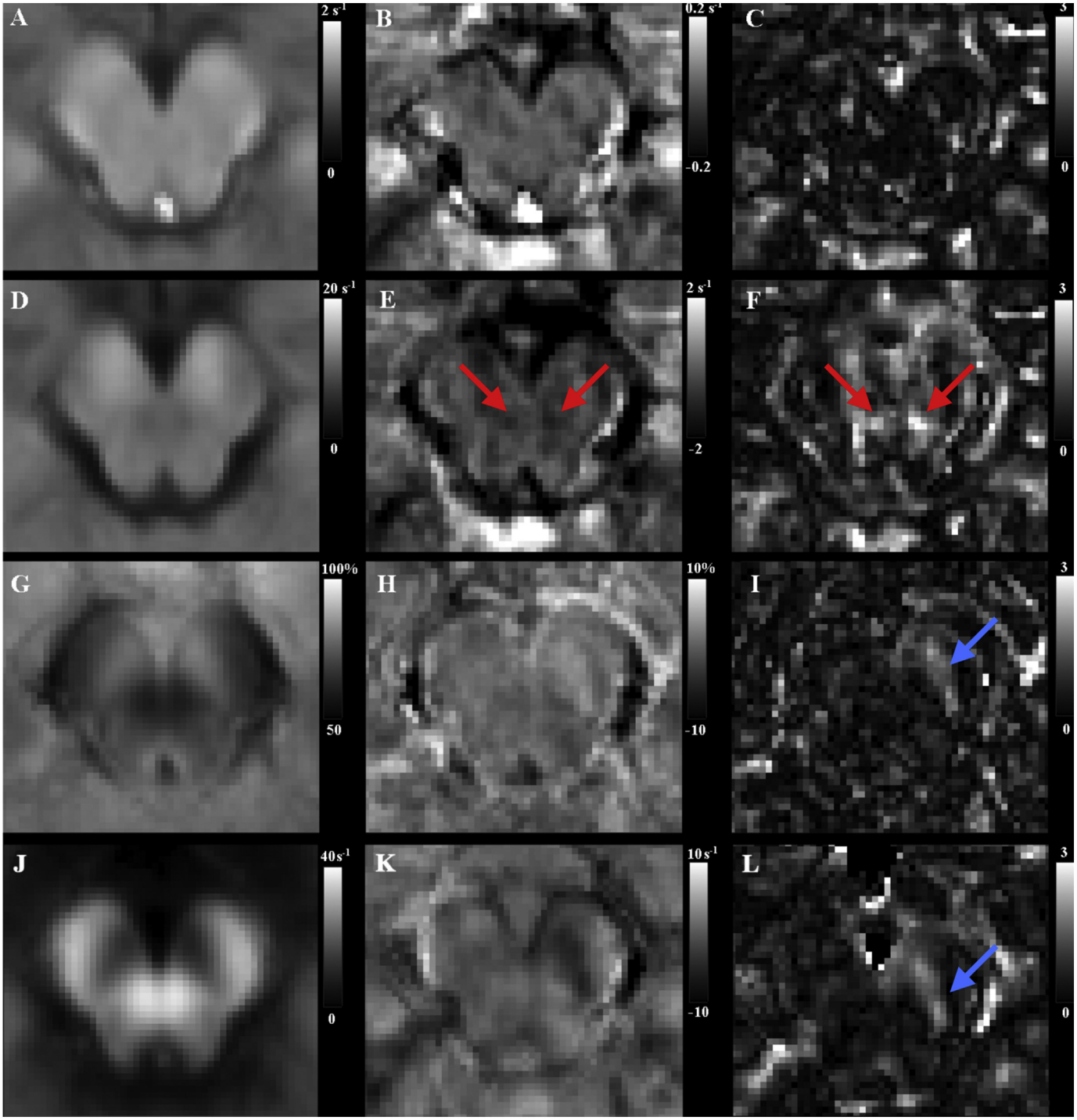

Fig. 3. Manually registered images of R1 and R2 relaxation rates, proton density and myelin. Analysis of R1 and R2 relaxation rates and proton density, where registration was concentrated at the brainstem at the level of the hippocampus. A) The average R1 relaxation rate of all subjects on a scale 0–2 s^{-1}, B) The average difference of the R1 relaxation rate of all narcolepsy patients and healthy controls on a scale -0.2–$0.2\,s^{-1}$. C) T-values representing the significance level of the difference on a scale 0–3. Similar images for R2 relaxation (D and F), proton density (G and I), and myelin (J and L). High significance levels were only observed in the R2 values at the location of the rostral reticular formation (shown with red arrows). Seeming differences in the substantia nigra were not statistically significant (blue arrows). (For interpretation of the references to color in this figure legend, the reader is referred to the web version of this article.)

compared to healthy controls. In Fig. 2B, it is seen that the significant deviant region in the reticular formation is more centrally located in the brainstem compared to the LC ROI (blue), but adjacent to the DRN (red). Fig. 2C shows a clear trend of R2 differences in the predefined locus coeruleus area.

In order to aid the localization of the observed R2 anomaly, we manually registered the slice covering the significant R2 deviation. Fig. 3 shows the average R1, R2, PD, and myelin values in this slice, the corresponding average differences, and the significance levels of the difference. In Fig. 3D and F, it is seen that the deviant area is located in the rostral reticular formation adjacent the superior cerebellar peduncle (red arrows). In supplementary Fig. S2 it is seen that the area with R2 deviation is not substantially extended in the superior-anterior direction, but mostly concentrated in a single slice of 5 mm thickness.

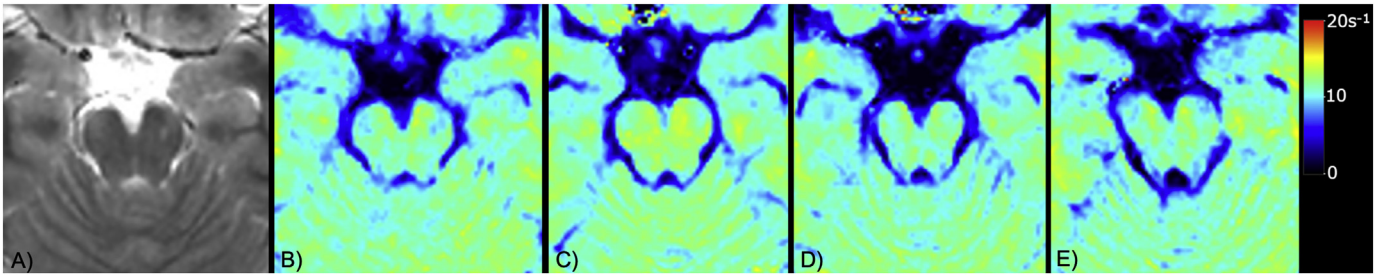

Fig. 4. R2 maps in individual subjects. The figure shows a reference T2 weighted image (A) and individual slices from two healthy controls (B, C) and two narcolepsy patients (D, E).

Inspecting the manually registered statistical maps, it seems like there are other areas with deviant structure in narcolepsy *e.g.,* the substantia nigra visible in the PD and myelin maps (blue arrows in Fig. 3I and L). However, these seeming deviations were not statistically significant when correcting for multiple comparison in the whole brainstem mask. Fig. 4 shows representative R2 images from two healthy participants and two narcolepsy patients.

3.3. Relation between R2 and clinical measures

R2-variance in our reticular formation area was explained by group *i.e.,* narcolepsy patients and healthy controls, $p < .001$, but not by any of the other clinical variables in the model. However, R2-variance in the predefined left LC was explained by total sleep duration: standardized coefficient for the regression, $\beta = 0.55$, T-value = 2.85, $p = .010$. R2-variance was not explained by sleep efficacy, cataplexy, age, sex, or group. Similar results were obtained for the right LC with $\beta = 0.57$, T-value = 2.87, $p = .009$ for sleep duration as predictor. In addition, group also explained part of the R2 variance in the right LC, $\beta = 0.59$, T-value = 2.16, $p = .043$. None of the predictors explained the R2 variance in DRN. No interaction effects were observed for the group*-clinical variable interaction in relation to any of the R2 measures.

3.4. Functional connections to OX signaling pathways

The R2 deviant area in the rostral reticular formation was functionally connected to several regions related to OX signaling pathways *e.g.,* the hypothalamus, ventral tegmental area, nucleus accumbens, amygdala, hippocampus, pallidum, and the thalamus, $p_{FDR} < 0.05$ (Fig. 5). We also observed significant connections to the parahippocampal gyrus and the cerebellum. Detailed reports of functional connectivity results are found in Table S1.

When comparing the functional connectivity between narcolepsy patients and healthy controls we found that patients with narcolepsy had higher connectivity between the identified area in the reticular formation and the supplementary motor area (SMA) and adjacent regions in the anterior cingulate cortex (ACC), cluster size $p_{FDR} = 0.025$, peak voxel coordinates = [−10 02 40]. Narcolepsy patients had lower connectivity between the identified area in the reticular formation and the right cerebellum and the right temporal fusiform cortex, $p_{FDR} = 0.023$, peak voxel coordinates = [30–36 -28] (Fig. 6).

4. Discussion

We examined brain structure in narcolepsy for structural differences related to loss of OX neuron signaling in narcolepsy. Our findings were threefold and summarized here.

1. We found that narcolepsy patients had significantly lower R2 levels localized to a small area of the brainstem in the rostral reticular formation.
2. Functional connectivity analysis showed that the identified area in the brainstem's rostral reticular formation was functionally connected to several areas involved in OX signaling *e.g.,* the hypothalamus, ventral tegmental area, nucleus accumbens, amygdala, hippocampus, pallidum, and the thalamus.
3. Narcolepsy patients had higher connectivity between the identified brainstem area and the SMA compared to their healthy peers and lower connectivity to the cerebellum and the temporal fusiform cortex.

R2 relaxation rate [R2 = 1/T2] is sensitive to the presence of metal ions, for example iron and copper, in tissue of both normal and diseased brains. The presence of metal ions produces T2 signal decay through its paramagnetic effect on susceptibility and microscopic field gradients (Ordidge et al., 1994). This property can be used to image neurons containing neuromelanin, which is a dark pigment synthesized from L-DOPA as a part of the dopamine metabolism. This is because neuromelanin chelates transition metal ions, including iron, copper, and zinc making it detectable in R2 images (Langley et al., 2017a; Langley et al., 2017b). Neuromelanin can be found in large quantities in specific nuclei of the brainstem such as the substantia nigra and the LC (Keren et al., 2015). Less commonly described are the pigmented nuclei surrounding the superior cerebellar peduncle whose function to a large extent is unclear (Fix, 1980; Ohm and Braak, 1988).

We identified a small area in the brain stem's rostral reticular formation near the superior cerebellar peduncle, which exhibited lower R2 levels in narcolepsy patients. The rostral reticular formation has no distinct cytoarchitectural boundaries, but includes architecturally defined nuclei, such as LC and DRN. Descriptions of the anatomical location of LC in standard coordinates are rather scattered (Liu et al., 2017) and only one study has reported a histologically validated LC location in the MNI coordinate system (Keren et al., 2015). According to the comprehensive review including 69 structural and functional MRI studies on LC by Liu et al. (Liu et al., 2017), the coordinates of our identified area fall within previously described LC locations (see Fig. 5 in (Liu et al., 2017)), but our brain stem area is more centrally located compared the predefined LC ROI based on Bär et al. (Bar et al., 2016), see Fig. 2B. Also in comparison with Keren et al. (Keren et al., 2015), the location in our study regarding the left-right and the superior-inferior directions is well in line with the histological coordinates but as seen in the axial slice in Fig. 1B, our identified area is located somewhat more anterior than previously described.

It should be noted that R2 increase does not only correspond to the presence of metal ions, even if its occurrence is more profound in regions with differences in magnetic susceptibility. It is also possible for myelin to enhance R2 relaxation rate due to its diamagnetism and water fraction, especially in white matter regions that has a high myelin and low iron content (Lee et al., 2011; Neema et al., 2007). In the current study, we examined myelin and proton density maps, but found no group differences suggesting that the observed differences are neuronal.

The functional connectivity analysis showed that our discovered region was functionally connected to the hypothalamus (Fig. 5). This finding supports involvement of parts of the reticular formation and the

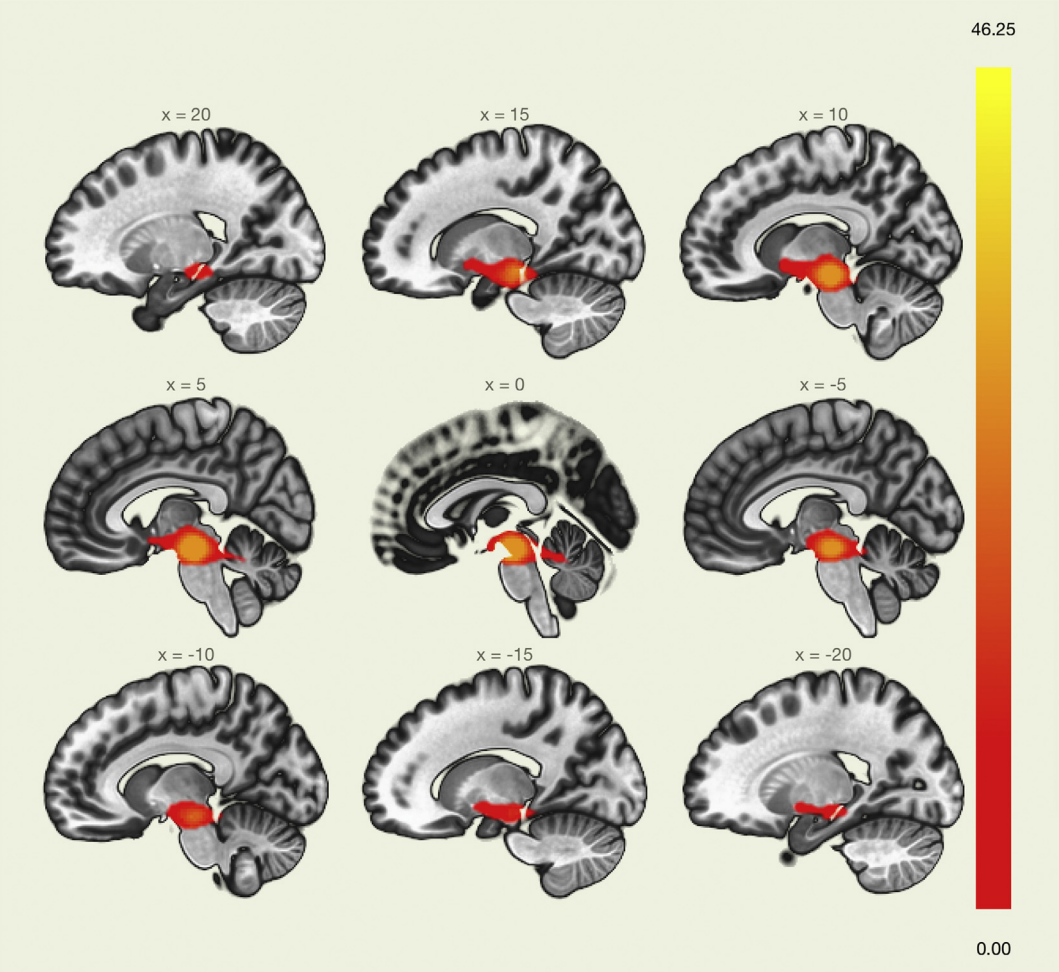

Fig. 5. Functional connectivity of the rostral reticular formation. The figure shows functional connectivity of the R2 deviant area in the rostral reticular formation adjacent to the superior cerebellar peduncle in nine sagittal slices representing all participants. The color bar indicates T-values for the statistics.

reticular activating system, especially when considering the connection between LC and the OX neurons of the hypothalamus (Aston-Jones et al., 1986; Dimitrov et al., 2013; Jones et al., 1977; Loughlin et al., 1986). Thus, our data indicate significant R2 differences between narcolepsy patients and healthy controls in an area in the brainstem's reticular formation, which might be related to lower levels of neuromelanin in the LC or other neuromelanin containing nuclei adjacent to the superior cerebellar peduncle.

When investigating R2 values in the predefined LC ROI we also found differences between narcolepsy patients and healthy controls, and objective measures of sleep duration the week before MRI predicted these R2 values. LC is the target of OX projections from the hypothalamus that promote arousal. LC is generally considered a wakefulness-promoting nucleus containing noradrenergic neurons, and its projections, while extensive, are also highly selective (Espana et al., 2005; Horvath et al., 1999). However, more recent research shows that inactivation of noradrenergic neurons of the LC causes fragmented sleep (Carter et al., 2010). This is corroborated by optogenetic studies, which show that restoring OX signaling specifically in the noradrenergic neurons of the LC of mice ameliorated fragmented sleep (Hasegawa et al., 2014), suggesting a role in sleep stabilization. It is also suggested that OX receptors in LC regulates rapid eye movement (REM) sleep and might be involved in the pathophysiology of narcolepsy (Bourgin et al., 2000).

Neuromelanin has also been proposed as a biomarker in neurodegenerative diseases, such as Parkinson's disease, where loss of dopaminergic cells in the substantia nigra overlaps with lower R2-levels (Langley et al., 2017b), presumably due to loss of neuromelanin. Thus, the LC has been implicated in neurodegeneration in Parkinson's disease and a similar decline in R2 can be seen in the LC of patients with Alzheimer's disease as well as mild cognitive impairment (Takahashi et al., 2015; Zarow et al., 2003). R2-levels have been observed to increase linearly with age also among adolescents (Clewett et al., 2016; Kumar et al., 2011) and are reversely correlated with an increased risk of dementia strengthening the idea of a neuro-protective role (Takahashi et al., 2015).

In addition to the LC, projections from the OX neurons of the hypothalamus also project to serotonergic neurons of the dorsal raphe and selective inhibition of these neurons produce cataplexy-like episodes in mice (Hasegawa et al., 2014). Like the LC, the dorsal raphe is situated in the brainstem and is also part of the reticular formation. In the *post hoc* analysis of R2 values in the predefined DRN ROI, we found significant group differences. However, unlike the LC, DRN does not contain any neuromelanin producing neurons (Kirby et al., 2003). As seen in Fig. 2B and C, the DRN ROI is adjacent to and at some parts overlapping with our identified area, but the ROI itself does not show many significantly different voxels even at low uncorrected thresholds. This suggests that the group difference in DRN is driven by the difference in the adjacent identified brainstem region. Taken together this suggests that our finding may not be localized in the dorsal raphe.

The aim of this study was to investigate potential microstructural differences in the brainstem between adolescents with narcolepsy and healthy controls. We found significant differences in R2 values in the rostral reticular formation adjacent to the superior cerebellar peduncle.

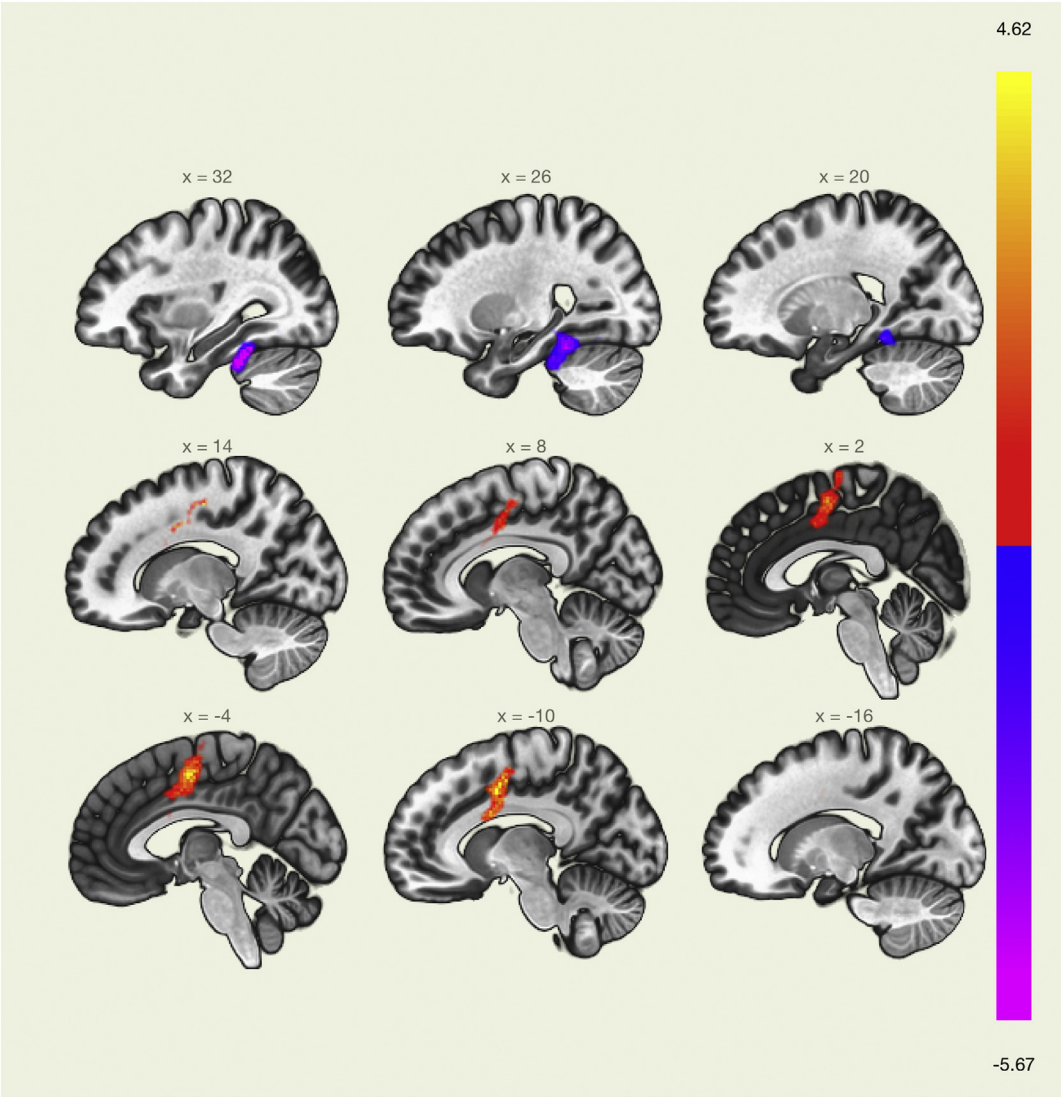

Fig. 6. Difference in functional connectivity between narcolepsy patients and healthy controls. Red/orange colored areas show regions where narcolepsy patients had higher connectivity than healthy controls. Blue/purple areas show regions where narcolepsy patients had lower connectivity than controls. The color bar indicates T-values for the statistics. (For interpretation of the references to color in this figure legend, the reader is referred to the web version of this article.)

Miscellaneous findings were differences in connectivity between this identified area and the SMA on the one hand and the cerebellum/temporal fusiform gyrus on the other. Imaging studies have found connections between nuclei in the proximity of the superior cerebellar peduncle *e.g.,* the pedunculopontine nucleus and the brain's motor regulation system including SMA and the cerebellum (Aravamuthan et al., 2007; Muthusamy et al., 2007), in line with previous cytoarchitectural studies (Rouiller et al., 1994). Of specific interest to the present study on narcolepsy patients with REM-sleep disorder, cerebellar-brainstem-frontal networks are involved in oculomotor control, and brainstem nuclei involved in sleep regulation and eye movements are found in the vicinity of each other (Lynch and Tian, 2006). The area here identified as SMA is identical with the supplementary eye field according to a meta-analysis on saccades by Jamadar et al. (Jamadar et al., 2013). A recent study by us also found brainstem-frontal eye fields connectivity differences between patients with periodic idiopathic hypersomnia, the Kleine-Levin Syndrome (KLS), and healthy controls (Engstrom et al., 2016). The eventual implications of the oculomotor system in patients with sleep disorders have to be evaluated in future studies.

5. Limitations

The major limitations of this study are the small sample size and the suboptimal voxel dimensions. The sequence we used for qMRI acquisition had high in-plane resolution (0.8 mm × 0.8 mm) but rather coarse slice thickness (5 mm). The sequence was optimized for clinical use with priority to reduce scanning time, however the acquired non-isotropic voxels could have aggravated the automated registration into standard MNI coordinates. Since brain stem nuclei are small in size, a slight mismatch in registration can make the anatomical localization of observed deviations somewhat uncertain. Our identified area with R2 differences between narcolepsy and controls seems to be more anteriorly located (Fig. 1B) compared to previous studies on LC (Keren et al., 2015; Liu et al., 2017). Signal differences in the applied non-isotropic voxels may have been affected by partial volume effects, reflecting differences in microstructure shape or volume in addition to differences in tissue properties.

6. Conclusion

In this study, we found that narcolepsy patients had significantly lower R2 levels localized to a small area of the brainstem in the rostral

reticular formation adjacent to the superior cerebellar peduncle. The connectivity analysis showed that this area was functionally connected to the OX signaling system. In conclusion, the observed R2 differences described in this paper could be due to lower levels of neuromelanin in the LC or other neuromelanin containing nuclei in the proximity of the superior cerebellar peduncle of narcolepsy patients.

Supplementary data to this article can be found online at https://doi.org/10.1016/j.nicl.2019.101875.

Acknowledgements

The Research Council of South East Sweden (FORSS-480551), the Knut and Alice Wallenberg foundation (KAW 2013.0076), and the Country council of Östergötland, Sweden (LIO-304651), are acknowledged for financial support of the study. Dr. Nataliya Zheliba is acknowledged for recruitment of patients in Östergötland. Henriettae Ståhlbrandt is acknowledged for radiological inspection of T1W images.

References

Aran, A., Einen, M., Lin, L., Plazzi, G., Nishino, S., Mignot, E., 2010. Clinical and therapeutic aspects of childhood narcolepsy-cataplexy: a retrospective study of 51 children. Sleep 33 (11), 1457–1464.

Aravamuthan, B.R., Muthusamy, K.A., Stein, J.F., Aziz, T.Z., Johansen-Berg, H., 2007. Topography of cortical and subcortical connections of the human pedunculopontine and subthalamic nuclei. Neuroimage 37 (3), 694–705.

Aston-Jones, G., Ennis, M., Pieribone, V.A., Nickell, W.T., Shipley, M.T., 1986. The brain nucleus locus coeruleus: restricted afferent control of a broad efferent network. Science 234 (4777), 734–737.

Bar, K.J., de la Cruz, F., Schumann, A., Koehler, S., Sauer, H., Critchley, H., et al., 2016. Functional connectivity and network analysis of midbrain and brainstem nuclei. Neuroimage 134, 53–63.

Blumberg, M.S., Coleman, C.M., Johnson, E.D., Shaw, C., 2007. Developmental divergence of sleep-wake patterns in orexin knockout and wild-type mice. Eur. J. Neurosci. 25 (2), 512–518.

Bourgin, P., Huitron-Resendiz, S., Spier, A.D., Fabre, V., Morte, B., Criado, J.R., et al., 2000. Hypocretin-1 modulates rapid eye movement sleep through activation of locus coeruleus neurons. J. Neurosci. 20 (20), 7760–7765.

Carter, M.E., Yizhar, O., Chikahisa, S., Nguyen, H., Adamantidis, A., Nishino, S., et al., 2010. Tuning arousal with optogenetic modulation of locus coeruleus neurons. Nat. Neurosci. 13 (12), 1526–1533.

Clewett, D.V., Lee, T.H., Greening, S., Ponzio, A., Margalit, E., Mather, M., 2016. Neuromelanin marks the spot: identifying a locus coeruleus biomarker of cognitive reserve in healthy aging. Neurobiol. Aging 37, 117–126.

Dauvilliers, Y., Baumann, C.B., Carlander, B., Bischof, M., Blatter, T., Lecendreux, M., et al., 2003. CSF hypocretin-1 levels in narcolepsy, Kleine-Levin syndrome, and other hypersomnias and neurological conditions. J. Neurol. Neurosur. Ps. 74 (12), 1667–1673.

Dergacheva, O., Yamanaka, A., Schwartz, A.R., Polotsky, V.Y., Mendelowitz, D., 2016. Direct projections from hypothalamic orexin neurons to brainstem cardiac vagal neurons. Neuroscience 339, 47–53.

Dimitrov, E.L., Yanagawa, Y., Usdin, T.B., 2013. Forebrain GABAergic projections to locus coeruleus in mouse. J. Comp. Neurol. 521 (10), 2373–2397.

Drissi, N.M., Szakacs, A., Witt, S.T., Wretman, A., Ulander, M., Stahlbrandt, H., et al., 2016. Altered brain microstate dynamics in adolescents with narcolepsy. Front. Hum. Neurosci. 10.

Engstrom, M., Landtblom, A.M., Karlsson, T., 2016. New hypothesis on pontine-frontal eye field connectivity in Kleine-Levin syndrome. J. Sleep Res. 25 (6), 716–719.

Espana, R.A., Reis, K.M., Valentino, R.J., Berridge, C.W., 2005. Organization of hypocretin/orexin efferents to locus coeruleus and basal forebrain arousal-related structures. J. Comp. Neurol. 481 (2), 160–178.

Fix, J.D., 1980. A melanin-containing nucleus associated with the superior cerebellar peduncle in man - cytomorphometric analysis. J. Hirnforsch. 21 (4), 429–436.

Frey, J.L., Heiserman, J.E., 1997. Absence of pontine lesions in narcolepsy. Neurology 48 (4), 1097–1099.

Hasegawa, E., Yanagisawa, M., Sakurai, T., Mieda, M., 2014. Orexin neurons suppress narcolepsy via 2 distinct efferent pathways. J. Clin. Invest. 124 (2), 604–616.

Horvath, T.L., Peyron, C., Diano, S., Ivanov, A., Aston-Jones, G., Kilduff, T.S., et al., 1999. Hypocretin (orexin) activation and synaptic innervation of the locus coeruleus noradrenergic system. J. Comp. Neurol. 415 (2), 145–159.

Hungs, M., Fan, J., Lin, L., Lin, X.Y., Maki, R.A., Mignot, E., 2001. Identification and functional analysis of mutations in the hypocretin (orexin) genes of narcoleptic canines. Genome Res. 11 (4), 531–539.

Jamadar, S.D., Fielding, J., Egan, G.F., 2013. Quantitative meta-analysis of fMRI and PET studies reveals consistent activation in fronto-striatal-parietal regions and cerebellum during antisaccades and prosaccades. Front. Psychol. 4, 749.

Jones, B.E., Halaris, A.E., Mcilhany, M., Moore, R.Y., 1977. Ascending projections of locus coeruleus in rat.1. axonal-transport in central noradrenaline neurons. Brain Res. 127 (1), 1–21.

Juvodden, H.T., Alnaes, D., Lund, M.J., Agartz, I., Andreassen, O.A., Dietrichs, E., et al., 2018. Widespread white matter changes in post-H1N1 patients with narcolepsy type 1 and first-degree relatives. Sleep 41 (10).

Keren, N.I., Taheri, S., Vazey, E.M., Morgan, P.S., Granholm, A.C.E., Aston-Jones, G.S., et al., 2015. Histologic validation of locus coeruleus MRI contrast in post-mortem tissue. Neuroimage 113, 235–245.

Khatami, R., Maret, S., Werth, E., Retey, J., Schmid, D., Maly, F., et al., 2004. Monozygotic twins concordant for narcolepsy-cataplexy without any detectable abnormality in the hypocretin (orexin) pathway. Lancet 363 (9416), 1199–1200.

Kirby, L.G., Pernar, L., Valentino, R.J., Beck, S.G., 2003. Distinguishing characteristics of serotonin and now serotonin-containing cells in the dorsal raphe nucleus: electrophysiological and immunohistochemical studies. Neuroscience 116 (3), 669–683.

Kumar, R., Delshad, S., Macey, P.M., Woo, M.A., Harper, R.M., 2011. Development of T2-relaxation values in regional brain sites during adolescence. Magn. Reson. Imaging 29 (2), 185–193.

Langley, J., Huddleston, D.E., Liu, C.J., Hu, X.P., 2017a. Reproducibility of locus coeruleus and substantia nigra imaging with neuromelanin sensitive MRI. Magn. Reson Mater. Phy. 30 (2), 121–125.

Langley, J., Huddleston, D.E., Sedlacik, J., Boelmans, K., Hu, X.P., 2017b. Parkinson's disease-related increase of T*(2)-weighted hypointensity in Substantia Nigra pars compacta. Mov. Disord. 32 (3), 441–449.

Lee, J., van Gelderen, P., Kuo, L.W., Merkle, H., Silva, A.C., Duyn, J.H., 2011. T-2*-based fiber orientation mapping. Neuroimage 57 (1), 225–234.

Lin, L., Faraco, J., Li, R., Kadotani, H., Rogers, W., Lin, X.Y., et al., 1999. The sleep disorder canine narcolepsy is caused by a mutation in the hypocretin (orexin) receptor 2 gene. Cell 98 (3), 365–376.

Liu, K.Y., Marijatta, F., Hammerer, D., Acosta-Cabronero, J., Duzel, E., Howard, R.J., 2017. Magnetic resonance imaging of the human locus coeruleus: a systematic review. Neurosci. Biobehav. R. 83, 325–355.

Loughlin, S.E., Foote, S.L., Grzanna, R., 1986. Efferent projections of nucleus locus-coeruleus - morphological subpopulations have different efferent targets. Neuroscience 18 (2) (307-&).

Lynch, J.C., Tian, J.R., 2006. Cortico-cortical networks and cortico-subcortical loops for the higher control of eye movements. Prog. Brain Res. 151, 461–501.

Medicine AAoS, 2005. International classification of sleep disorders. In: Diagnostic Coding Manual. American Academy of Sleep Medicine, Chicago, Illinois, USA.

Medicine AAoS, 2014. International classification of sleep disorders. In: Diagnostic Coding Manual. American Academy of Sleep Medicine, Chicago, Illinois, USA.

Menzler, K., Belke, M., Unger, M.M., Ohletz, T., Keil, B., Heverhagen, J.T., et al., 2012. DTI reveals hypothalamic and brainstem white matter lesions in patients with idiopathic narcolepsy. Sleep Med. 13 (6), 736–742.

Muthusamy, K.A., Aravamuthan, B.R., Kringelbach, M.L., Jenkinson, N., Voets, N.L., Johansen-Berg, H., et al., 2007. Connectivity of the human pedunculopontine nucleus region and diffusion tensor imaging in surgical targeting. J. Neurosurg. 107 (4), 814–820.

Neema, M., Stankiewicz, J., Arora, A., Dandamudi, V.S.R., Batt, C.E., Guss, Z.D., et al., 2007. T1-and T2-based MRI measures of diffuse gray matter and white matter damage in patients with multiple sclerosis. J. Neuroimaging 17, 16s–21s.

Ohm, T.G., Braak, H., 1988. The pigmented subpeduncular nucleus - a neuromelanin-containing nucleus in the human pontine tegmentum - morphology and changes in Alzheimers-disease. Acta Neuropathol. 77 (1), 26–32.

Ordidge, R.J., Gorell, J.M., Deniau, J.C., Knight, R.A., Helpern, J.A., 1994. Assessment of relative brain Iron concentrations using T-2-weighted and T-2(asterisk)-weighted Mri at 3-tesla. Magn. Reson. Med. 32 (3), 335–341.

Peraita-Adrados, R., Garcia-Penas, J.J., Ruiz-Falco, L., Gutierrez-Solana, L., Lopez-Esteban, P., Vicario, J.L., et al., 2011. Clinical, polysomnographic and laboratory characteristics of narcolepsy-cataplexy in a sample of children and adolescents. Sleep Med. 12 (1), 24–27.

Rouiller, E.M., Liang, F., Babalian, A., Moret, V., Wiesendanger, M., 1994. Cerebellothalamocortical and pallidothalamocortical projections to the primary and supplementary motor cortical areas: a multiple tracing study in macaque monkeys. J. Comp. Neurol. 345 (2), 185–213.

Silber, M.H., Krahn, L.E., Olson, E.J., 2002. Diagnosing narcolepsy: validity and reliability of new diagnostic criteria. Sleep Med. 3 (2), 109–113.

Szakacs, A., Darin, N., Hallbook, T., 2013. Increased childhood incidence of narcolepsy in western Sweden after H1N1 influenza vaccination. Neurology 80 (14), 1315–1321.

Takahashi, J., Shibata, T., Sasaki, M., Kudo, M., Yanezawa, H., Obara, S., et al., 2015. Detection of changes in the locus coeruleus in patients with mild cognitive impairment and Alzheimer's disease: high-resolution fast spin-echo T1-weighted imaging. Geriatr Gerontol Int 15 (3), 334–340.

Thannickal, T.C., Moore, R.Y., Nienhuis, R., Ramanathan, L., Gulyani, S., Aldrich, M., et al., 2000. Reduced number of hypocretin neurons in human narcolepsy. Neuron 27 (3), 469–474.

Wada, M., Mimura, M., Noda, Y., Takasu, S., Plitman, E., Honda, M., et al., 2019. Neuroimaging correlates of narcolepsy with cataplexy: a systematic review. Neurosci. Res. 142, 16–29.

Warntjes, J.B., Leinhard, O.D., West, J., Lundberg, P., 2008. Rapid magnetic resonance quantification on the brain: optimization for clinical usage. Magn. Reson. Med. 60 (2), 320–329.

Warntjes, M., Engstrom, M., Tisell, A., Lundberg, P., 2016. Modeling the presence of Myelin and Edema in the brain based on multi-parametric quantitative MRI. Front. Neurol. 7, 16.

Warntjes, J.B.M., Persson, A., Berge, J., Zech, W., 2017. Myelin detection using rapid quantitative MR imaging correlated to macroscopically registered luxol fast blue-stained brain specimens. AJNR Am. J. Neuroradiol. 38 (6), 1096–1102.

Weng, H.H., Chen, C.F., Tsai, Y.H., Wu, C.Y., Lee, M., Lin, Y.C., et al., 2015. Gray matter atrophy in narcolepsy: an activation likelihood estimation meta-analysis. Neurosci.

Biobehav. Rev. 59, 53–63.
Whitfield-Gabrieli, S., Nieto-Castanon, A., 2012. Conn: a functional connectivity toolbox for correlated and anticorrelated brain networks. Brain Connect. 2 (3), 125–141.
Witt, S.T., Drissi, N.M., Tapper, S., Wretman, A., Szakacs, A., Hallbook, T., et al., 2018. Evidence for cognitive resource imbalance in adolescents with narcolepsy. Brain Imag. Behav. 12 (2), 411–424.
Zarow, C., Lyness, S.A., Mortimer, J.A., Chui, H.C., 2003. Neuronal loss is greater in the locus coeruleus than nucleus basalis and substantia nigra in Alzheimer and Parkinson diseases. Arch. Neurol.-Chic. 60 (3), 337–341.